

MULTISCALE EXPERIMENTS AND MODELING IN BIOMATERIALS AND BIOLOGICAL MATERIALS

Single Chain Hydration and Dynamics of Mussel-Inspired Soybean-Based Adhesive

ABDOL HADI MOKARIZADEH $^{\circ}$, NITYANSHU KUMAR $^{\circ}$, ABRAHAM JOY $^{\circ}$, ALI DHINOJWALA $^{\circ}$, and MESFIN TSIGE $^{\circ}$ 1,2

1.—School of Polymer Science and Polymer Engineering, The University of Akron, Akron, OH 44325, USA. 2.—e-mail: mtsige@uakron.edu

Mussels, which are marine creatures, stick strongly to various substrates underwater using foot proteins rich in amino acids like L-3,4-dihydroxyphenylalanine (DOPA). This stimulates the synthesis of catechol-containing polymers that possess strong underwater adhesion; consequently, the mechanism is ascribed solely to catechol functionality. However, polymers' adsorption state and hence adhesion are a function of hydration and intramolecular interactions, insights into which are lacking. Here, we investigate dilute solution behavior of polyester adhesive polymers containing linoleamide group for hydrophobicity (H) and catechol group to mimic DOPA functionality (D). Higher D unit content containing polymers hydrate more through catechol hydroxyl groups and explore a wide range of conformational space. Neither ester oxygen nor nitrogen atoms in the backbone show any hydration. Interestingly, all polymers show hydrophobic collapse with extent/ structure depending upon content of H unit. Hydrophobic collapse due to enthalpic interactions and chain entropy enhancement via catechol group provide insights into polymers' un-adsorbed state.

INTRODUCTION

Aquatic lifeforms include creatures like mussels, barnacles and sandcastle worms that form strong interfacial bonds to various substrates underwater using biological adhesives. $^{1-2}$ Among them, mussel uses foot proteins (Mfp-3F, -3S, -5) rich in DOPA to adhere in diverse ways. $^{3-4}$ DOPA contains a catechol binding group capable of forming multiple hydrogen bonds to oxide surfaces, chelating with metal oxide and metallic surfaces and engaging in hydrophobic interactions to non-polar surfaces. Single-molecule pull-off force measurements of catechol group with a variety of substrates have elucidated, to some extent, the bonding mechanism through comparisons of binding energies. $^{8,11-13}$ For example, the low adhesion values of catechol on SiO₂ and Al₂O₃ surfaces suggested the mode of

interaction to be solely hydrogen bonding whereas on TiO2 surfaces the binding energies point toward the occurrence of monodentate, bidentate and chelated coordination compounds. 8,12 Furthermore, several density function theory (DFT) and molecular dynamics (MD) simulation studies have explored the orientation and binding strengths of catechol molecule with a variety of substrates in dry and underwater conditions. ^{14–18} These insights led to the perception that for catechol (or DOPA) containing proteins or polymers the adhesion is entirely governed by DOPA and the DOPA sticks to all surfaces. However, both perceptions were proved wrong in a seminal work by Israelachvili et al. 7 The authors demonstrated that adhesion on a hydrophobic surface was highest for protein containing a higher content of hydrophobic groups but not the DOPA, highlighting the role of hydrophobic residues. Furthermore, on hydrophilic surfaces the interaction of DOPA can easily be frustrated by changing the hydrogen bond acceptor distance as the catechol unit can only form multiple hydrogen bonds in vicinities of a particular geometry.⁵

Abdol Hadi Mokarizadeh and Nityanshu Kumar have contributed equally to the work.

(Received February 22, 2021; accepted May 28, 2021)

Published online: 21 June 2021

For adhesive polymers, demarcating the role of catechol functionality is more complex as it can influence the cohesive strength of a polymer to a great extent by forming interchain hydrogen bonds and self-crosslinking via oxidation. 19-21 This poses a challenge to understanding any measured adhesion values as the adhesion depends upon both the interfacial interactions and bulk dissipation.²² Recently, the strategy to keep the bulk contributions constant for catechol-containing mussel-inspired polyester adhesive and their interfacespecific characterization demonstrated the interplay of polymer hydrophobicity and catechol functionality on a hydrophilic surface as well.²³ The hydrophobic part of the adhesive polymer was believed to remove water from the interface with the catechol functionality engaging in multi-modal bonding with the hydrophilic surface. Even though both the polymer hydrophobicity and catechol functionality played a role in observed high underwater adhesion, it is difficult to delineate the contributions. Insights such as entropy loss on adsorption, intramolecular interactions and hydration affinity of the adhesive polymer as well as the availability of catechol groups to engage in enthalpic interactions for water surrounded collapsed polymers are critical but are lacking in experiments. This motivated us to explore the behavior of these complex mussel-inspired polymers (MIPs) using atomistic simulations to understand their working mechanism.

Our focus in the present study is to have a better understanding of the solution properties of MIPs, while their adhesion properties in the presence of water will be investigated in the future. Hence, we performed single-chain MD simulations of homoco-polyesters with varying contents hydrophobic soybean and catechol-containing monomers in water. The radius of gyration, chain end-toend distance and solvent-accessible surface area distributions demonstrated the structural behavior of these MIPs. Furthermore, pair correlations of polar atoms of polymer chain with water molecules established the hydration affinity of various parts in the polymer chain. The chain and monomer relaxation times are related to the structural information of these MIPs. The role of hydrophobic interactions in chain collapse and catechol moieties in hydrogen bonding is conspicuous and has competing effects on polymer structure and dynamics.

METHODS

The controlled design/synthesis of MIP adhesives by Kaur and Narayan et al. with vigilant characterization and intriguing results inspired us to explore the behavior of MIPs underwater using MD simulations.^{23,24} Their MIPs contain three types of monomers with specific pendant groups and functionality, namely, the hydrophobic (linoleamide, major part of soybean), catechol and coumarin unit, connected through ester bonds.

Monomer with a linoleamide pendant group (H) (Fig. 1a) imparts the hydrophobicity and lowers the polymers' glass transition temperature and viscosity. Monomer with a catechol pendant group (representative of DOPA) (D) (Fig. 1b) is believed to enhance the adhesion of these polymers to different substrates. Finally, the monomer with the coumarin pendant group is incorporated in the co-polyester to photo-crosslink the polymer chains and hence enhance cohesive strength. The coumarin unit is dropped as it will only make computations expensive and is merely added to crosslink chains in experiments. Figure 1a and b shows the chemical structure of the H and D monomers, while Fig. 1c represents the groups used to terminate the polymer chains.

Simulation Methodology

Initial atomic structure of D and H units was determined and employed to build homo-polymers (referred hereafter as DDD and HHH) and tri-copolymers (DHD and HDH) using Materials Studio package.²⁵ Strictly speaking, they are oligomers rather than polymers but referred to as polymers since we are not investigating the effect of molecular weight. Each polymer chain was solvated with 8000 water molecules using the PACKMOL package to generate initial simulation systems.²⁶ The optimized potentials for liquid simulations all-atom (OPLS-AA) force field was employed to describe the bonded and non-bonded interactions (van der Waals and coulombic) between the polymer atoms. $^{27-28}$ The SPC/E model was used for water, where the SHAKE algorithm was employed to fix the bond length and angle.²⁹ Interaction parameters between polymer and water atoms were calculated using the arithmetic combination rules. All MD simulations were performed using the open-source LAMMPS software package.³⁰ Periodic boundary conditions were used along with the three directions: x, y and z. The real space interactions (Lennard-Jones 6-12 and coulombic) were calculated with a cutoff of 12 Å. Long-range electrostatic interactions were calculated in reciprocal space using the particle-particle particle-mesh (PPPM) algorithm with an accuracy of 10^{-4} . The initial systems were first equilibrated in NPT ensemble (Nose/Hoover thermostat and barostat) for 2 ns at 298 K and 1 atm followed by an 8 ns run in a NVT ensemble to allow configurational equilibration evaluated using radius of gyration as a metric. Production runs of 50 ns were performed for each of the systems with data stored every 2 ps throughout the run. The molecular weights of the MIPs, HHH, DDD, HDH and DHD, are 1603, 1308, 1505 and 1406 g/mol. respectively.

Fig 1. Chemical structures of (a) H and (b) D monomer unit used to create mono- and co-polyesters with end group termination of a (c) hydroxyl and hydrogen.

RESULTS

The hydration behavior of a single polymer chain relies on parameters such as polymer interactions and solvent quality. The polymer chain size is directly affected by the hydration behavior, and the radius of gyration directly correlates with the extent of collapse or hydration.³¹ Radius of gyrations is defined as shown in Eq. 1:

$$R_g^2 = \frac{\sum_{i=1}^{N} m_i (r_i - r_{cm})^2}{\sum_{i=1}^{N} m_i}$$
 (1)

where N and r_{cm} are the number of atoms and the center of mass of the polymer molecule, respectively, and m_i and r_i are the mass and the position of atom i, respectively. Figure 2a and b shows the time evolution of the radius of gyration (normalized by molecular weight) and the corresponding probability distributions for the whole 50 ns of the production run. The radius of gyration is normalized with respect to the molecular weight of corresponding polymer chain to account for the variation in size of pendant groups among the different polymer chains. The fact that each of the radius of gyration values fluctuates around a stable value and does not show any significant drift with time (Fig. 2a) confirms that the systems have reached equilibrium before the production runs.

The MIPs with higher D content (DDD and DHD) show higher R_g accompanied by higher fluctuations compared to that of HHH and HDH (Fig. 2a). Figure 2b shows the probability distributions of the normalized radius of gyrations. The average values with standard deviations for the distributions are presented in Table I. Both the distributions and the numbers clarify the trend in R_g : DDD > DHD > HDH > HHH as well as in their standard deviations: DDD \approx DHD > HDH > HHH. This trend in R_g values should not be correlated with the trend in

their standard deviations as the latter is a function of the number of conformations or the broadness in the probability distributions. To investigate the implications of the standard deviations, conformation landscapes in the form of a scatter plot for each of the MIP chains are shown in Fig. 2c, where both R_g and the end-to-end distance $(R_{\rm ee})$ have been considered. Clearly, in accordance with the standard deviation numbers, the scatter plots for DDD and DHD chains are more compared to those of HHH and HDH chains. Interestingly, the HDH and DHD scatter plots show two major populations of $R_{\rm ee}^2$ for similar R_g values. Among these, one population has a $R_{\rm ee}^2$ close to zero.

Another critical aspect of hydration is the polymer surface area accessible to surrounding solvent molecules. Figure 2d shows the probability distributions of the solvent-accessible surface area (SASA) of the MIPs to water molecules. A probe sphere of radius 1.4 A, to mimic a water molecule, was used to calculate the SASA. Chain size variability is accounted for by normalizing the SASA values to the number of carbon atoms in the corresponding MIP chains. Average SASA values with their standard deviations are reported in Table I and are found to correlate with normalized ${<\!R_g}^2\!>$ values. The one anomaly we observed is that for DHD, SASA distribution is slightly broader compared to that for DDD (Fig. 2d), which is also evident in their standard deviation numbers Table I.

We would point out here that despite having so many polar groups along the backbone of these MIPs, these polymers are experimentally known to be insoluble in water or uptake a minimal amount of water. This motivated us to investigate the interactions and possibility of hydrogen bonding of the polar groups in the MIPs with water molecules. Furthermore, Fig. 2c shows that the chain size and conformations vary noticeably with the content of

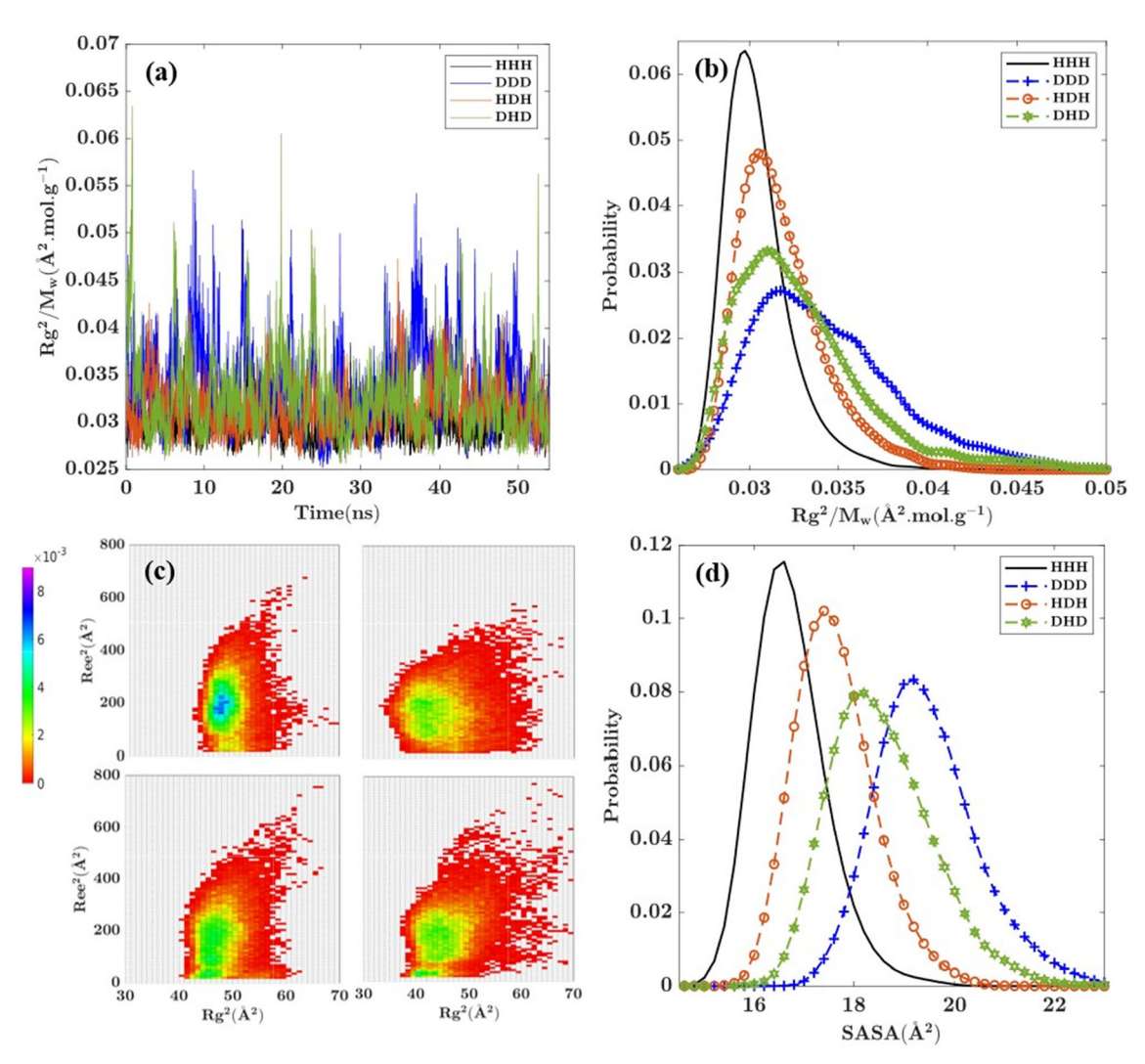


Fig 2. (a) Trajectory of molecular weight normalized radius of gyration squared, (b) distribution of the normalized radius of gyration squared, (c) conformation probability distribution with respect to radius of gyration squared and end-to-end distance squared of HHH (top left), DDD (top right), HDH (bottom left), DHD (bottom right) and (d) distribution of solvent-accessible surface area normalized with respect to the corresponding number of carbons of each polymer chain

Table I. Time-averaged radius of gyration and SASA including their corresponding standard deviations for the MIPs

Polymer	$< R_g^2 > (\mathring{A}^2 \text{ mol } g^{-1})$	${\sigma_{Rg}}^2$	$<$ SASA > $(\mathring{\mathrm{A}}^2)$	$\sigma_{\rm SASA}$
ННН	0.03001	0.0019	16.48	0.734
DDD	0.0338	0.0041	19.20	1.019
HDH	0.0313	0.0025	17.37	0.797
DHD	0.0325	0.0040	18.31	1.029

the D or H monomer. The presence of any water structure around the polar group and their interactions can be commented upon by evaluating the density of water molecules along the radial direction to the polar groups using the pair correlation function given by Eq. 2, 32

$$g(\mathbf{r}) = \frac{V}{4\pi r^2 N^2} \left\langle \sum_{i}^{N} \sum_{j\neq i}^{N} \delta(\mathbf{r} - \mathbf{r}_{ij}) \right\rangle$$
 (2)

where V is the total system volume, N is the number of unique pairs of atoms ij, and δ is the Kronecker delta function.

Figure 3 shows the pair-correlation distributions of the water oxygen atom with electronegative atoms of the MIPs to check the formation of hydrogen bonds through water hydrogen atoms. All the distributions are averaged for the last 20 ns of simulation time. At longer distances, the g(r) value for all the curves saturates to 1 as expected (not shown in the curves to focus on the key features such as peaks and valleys). Pair correlation distributions of chain-end hydroxyl oxygen atoms, catechol hydroxyl oxygen atoms (of D part) and carbonyl oxygen atoms of backbone/side chains with water oxygen atoms show the depletion of the first hydration shell at ~ 3.5 Å, pointing toward the formation of hydrogen bonds for all the MIPs, 33-34 whereas the pair correlations of the amide nitrogen atoms and the ester oxygen atoms of the MIP backbone with water oxygen atoms show that the location of the peak of the first hydration shell at ~4.8 Å with depletion at ~ 5.5 Å, pointing toward minimal water ordering and absence of hydrogen bonding. Also, it is clear from Fig. 3 that all these polymer chains show the highest first pair correlation peak intensity for the oxygen atom of the chain-end hydroxyl

group followed by the hydroxyl oxygen atom of catechol units (except for the HHH case where the catechol unit is absent) and then the oxygen of carbonyl groups in the backbone or side chains. Interestingly, water-polymer polar atom pair correlation distribution comparison (SI Fig. 1c) shows that the hydrogen bonding of water molecules with carbonyl oxygen is less prominent in HHH polymer compared to the MIPs with D content, as evident by the first peak intensity.

To quantify the hydration ability of the polar groups, the numbers of hydrogen bonds per functional group for all the systems are reported in Table II. Hydrogen bond between the different polar groups was calculated using the geometric criterion proposed by Luzar and Chandler. The cutoff on donor oxygen—acceptor oxygen distance is set to be < 3.5 Å with the cutoff on the acceptor hydrogen—acceptor oxygen—donor oxygen angle set to be < 30 degrees. All chains have the same number of carbonyl oxygen and one hydroxyl groups at the end. The number of catechol oxygens differs based on the content of the D unit in MIPs. The total number of hydrogen bonds with water molecules

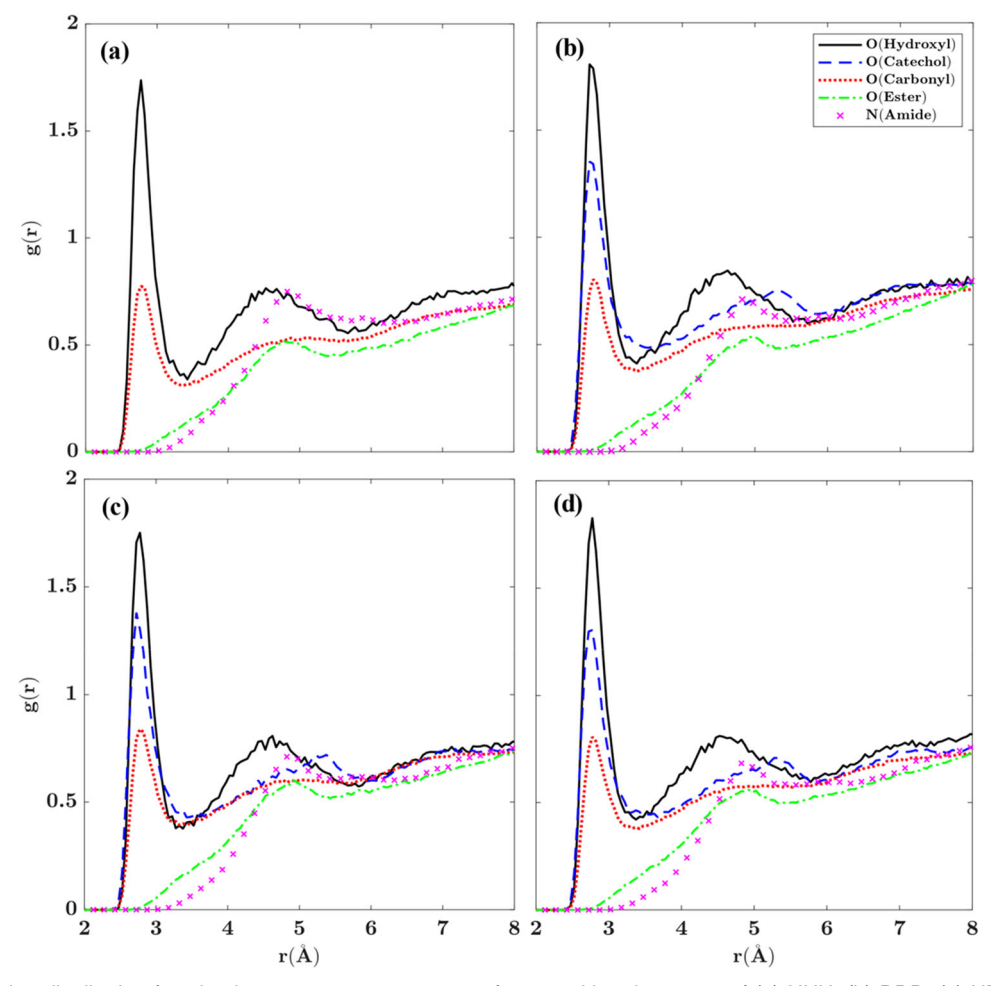


Fig 3. Pair correlation distribution function between an oxygen atom of water with polar atoms of (a) HHH, (b) DDD, (c) HDH, (d) DHD. In all panels, the oxygen of hydroxyl is shown as a solid line, oxygen of catechol as a dashed line, oxygen of carbonyl as a dotted line, oxygen of ester as a dashed-dotted line and nitrogen with x symbols.

Table II. Time-averaged number of water-polymer intermolecular and polymer-polymer intramolecular hydrogen bonds

<u>-</u>	Water-polymer intermolecular			Polymer-polymer intramolecular	
Polymer	Carbonyl oxygen	Hydroxyl oxygen	Catechol oxygen	Total	Hydroxyl-hydroxyl and hydroxyl- oxygen
HHH DDD	0.6875 0.6996	1.5450 1.7821	- 1.2357	7.7325 15.4927	$0.0558 \\ 0.00711$
HDH DHD	0.6990 0.7572 0.6600	1.6862 1.6862	1.2575 1.1184	$ \begin{array}{c} 15.4327 \\ 11.0212 \\ 14.3366 \end{array} $	0.00711 0.01873 0.0068

Each number is normalized with respect to the number of corresponding functional groups in the polymer chain. The total number is calculated by summation of the multiplication of average intermolecular hydrogen bonds with corresponding functional groups in the polymer chain

increases with content of the D unit. In addition to the intermolecular interactions, intramolecular interactions can play a critical role in hydration of the MIPs. Table II also contains the summary of the time-averaged number of intramolecular hydrogen bonds between two hydroxyl groups as well as between a hydroxyl group and an oxygen atom of a polymer chain. Time-averaged intramolecular hydrogen bonds are found to be much smaller than unity. These small values reveal that intramolecular hydrogen bonding happens less frequently compared to hydrogen bonding between water and the polymers. Furthermore, we observe that intramolecular hydrogen bonds increase with the increase in H content in the MIPs. The pair correlation between the carbonyl oxygen atom and chain-end hydroxyl group (SI, Fig. 2a) shows a peak corresponding to hydrogen bonding only for the case of HHH polymer. Furthermore, the pair correlation between the chain-end hydroxyl oxygen atom and catechol group oxygen atom shows the strongest peak for DHD followed by DDD polymer while absent for the HDH case. These MIPs contain a significant number of hydrophobic groups in the backbone as well as in the H pendant unit. The hydrophobic groups engage in van der Waals interactions and result in collapse of hydrophobic moieties together.³⁵ Furthermore, this could be the reason why these MIPs have low water retention capabilities.

To shed light on the possibility of hydrophobic intramolecular interactions, representative snapshots of the MIPs after equilibration are shown in Fig. 4. The snapshots show backbone atoms in gray, linoleamide side chain in blue and DOPA inspired group in red color for ease of visualization. It is clear from Fig. 4a that the hydrophobic side-chain segment of the H unit tends to align parallel to another side-chain segment of the H unit or the hydrophobic segment of the backbone. For HDH polymer, the hydrophobic segments of two H units interact and result in the collapse of the polymer chain with the

center catechol group of D unit exposed to water on the other side of the collapse, as shown in Fig. 4b. Figure 4c shows that the two D units are exposed to the water on the two sides of the polymer chain, with the hydrophobic segment of the H unit passing in between. For the polymer with all D units in Fig. 4d, the catechol moieties are again exposed to water, with the CH_2 segments of the backbone passing in between those groups. The intriguing structural arrangement of these MIPs with different D or H unit contents can have drastic consequences on the chain dynamics.

To explore the dependence of hydration behavior on chain size, we plot SASA and the average number of polymer-water hydrogen bonds as a function of R_g^2 and $R_{\rm ee}^2$ using scatter plots in Fig. 5a and b. Figure 5a shows that SASA increases with an increase in R_g and has no dependence on $R_{\rm ee}$. MIPs with higher content of D unit (DDD and DHD) have higher SASA corresponding to higher R_g values. Furthermore, Fig. 5b shows that the number of water-polymer hydrogen bonds is insensitive to the change in SASA and broadness in R_g versus $R_{\rm ee}$ scatter plots depicted by the constant hydrogen bonding value throughout the scatter plots. These striking observations require attention and will be discussed.

After a thorough structural analysis, we now present the segment and chain dynamics for these MIPs. Relaxation times for MIP chains are calculated using end-to-end distance autocorrelation function (ACF) given by Eq. 3:

$$ACF(t) = \frac{\langle R(t).R(0) \rangle}{\langle R(0).R(0) \rangle}$$
 (3)

where R(0) and R(t) are the end-to-end distance between two ends of the backbone at time 0 and t. The autocorrelation function is calculated and timeaveraged for >40 ns. To obtain the end-to-end orientation relaxation times, the auto-correlation

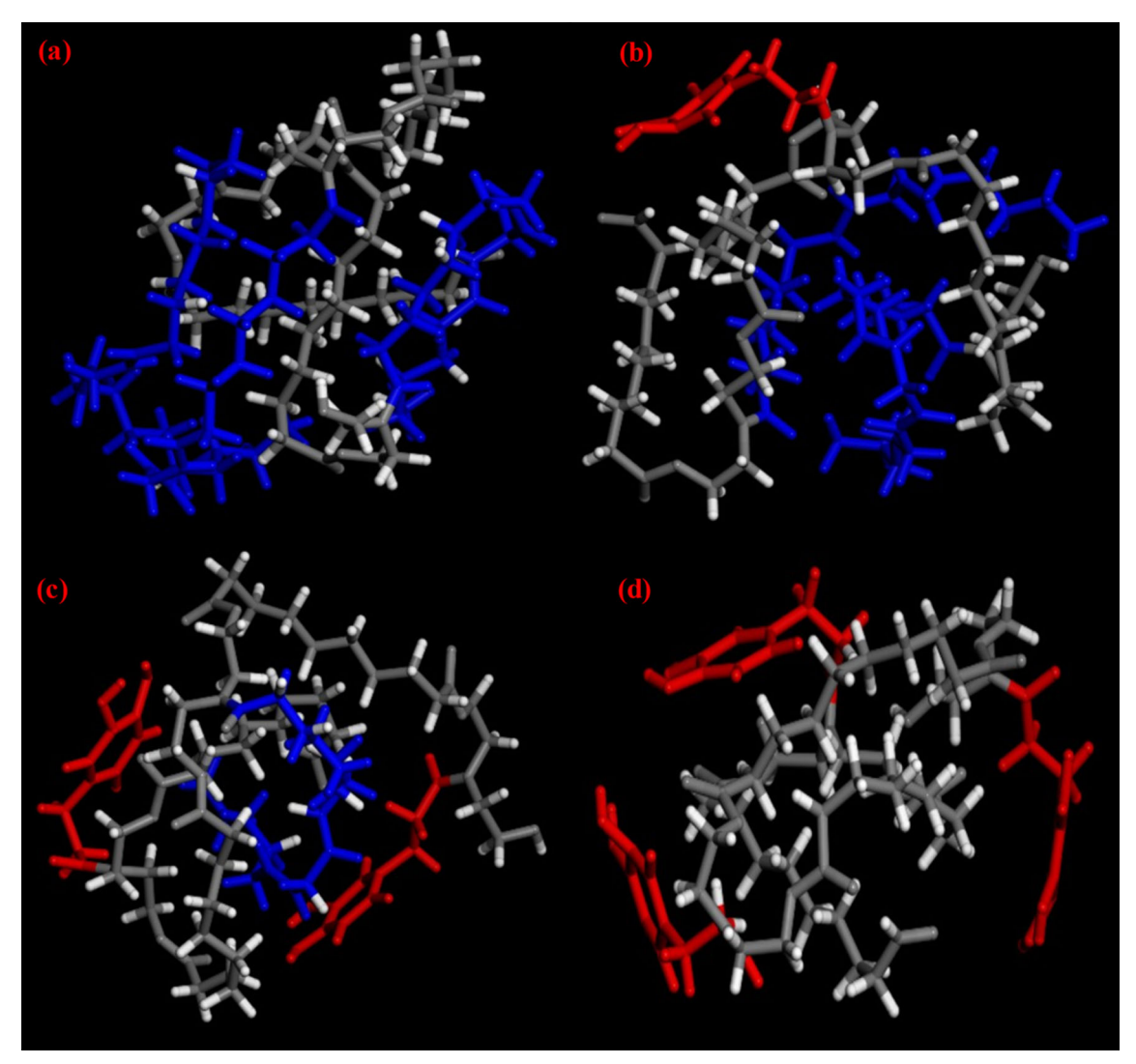


Fig 4. Representative snapshot of the chains of (a) HHH, (b) HDH, (c) DHD, (d) DDD. Backbone, soybean side groups and catechol groups are shown in gray, blue and red, respectively. Water has been omitted from the snapshots for clear visualization of MIP structure (Color figure online).

curves shown in Fig. 6a are first fitted with the Kohlrausch–Williams–Watts (KWW) function given by Eq. 4:³⁶

$$ACF(t) = A * exp \left[-\left(\frac{t}{\tau_{www}}\right)^{\beta} \right]$$
 (4)

where A is the pre-factor, which is responsible for relaxation at short times, τ_{www} is the KWW-relaxation time, and β is the degree of deviation from the Debye ideal model. The relaxation time of the chain is then computed by integrating the fitted KWW function using Eq. 5:

$$\tau = \int_{0}^{\infty} A * exp \left[-\left(\frac{t}{\tau_{www}}\right)^{\beta} \right] dt = \frac{A \cdot \tau_{www}}{\beta} \Gamma\left(\frac{1}{\beta}\right) \quad (5)$$

where Γ is the gamma function.

From Fig. 6a, it is evident that the DDD polymer relaxes quickly as it has the fastest decaying ACF. Further observations of the dynamics are rather tricky, and decay values are needed for comparison. Thereby, the relaxation time of the chains is calculated and reported in (SI, Table I). Accordingly, the relaxation time of DDD is 646.9 ± 1.4 ps, which decays faster than other polymers, while HDH has the slowest dynamics with $\tau = 925.81 \pm 1.5$ ps, and it is followed by HHH ($\tau = 851.7 \pm 1.8$ ps) and DHD $(\tau = 832.7 \pm 2.0 \text{ ps})$ single chains. In SI, Fig. S3a,b, orientational dynamics of each part of the backbone corresponding to the catechol or soybean side groups are shown, respectively. Also, KWW fitting values are depicted in (SI, Table II). In all cases, the first backbone corresponding to that of the hydroxyl end group has faster dynamics than the backbone at the other end with carbonyl oxygen as a result of monomer position relative to the ends.

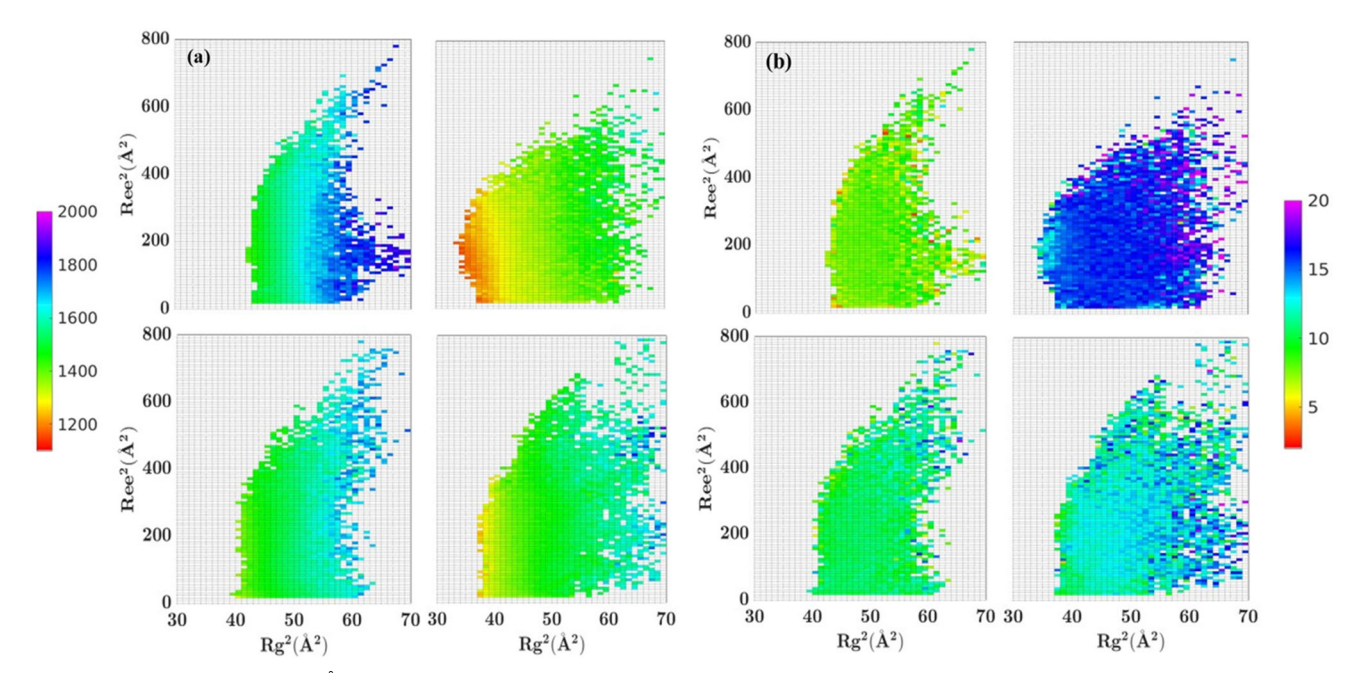


Fig 5. Scatter plots of (a) SASA (Å²), (b) total number of water-polymer hydrogen bonds, with respect to R_g^2 and R_{ee}^2 of the polymer chain. The figure for each group corresponds to the HHH (top left), DDD (top right), HDH (bottom left) and DHD (bottom right) case.

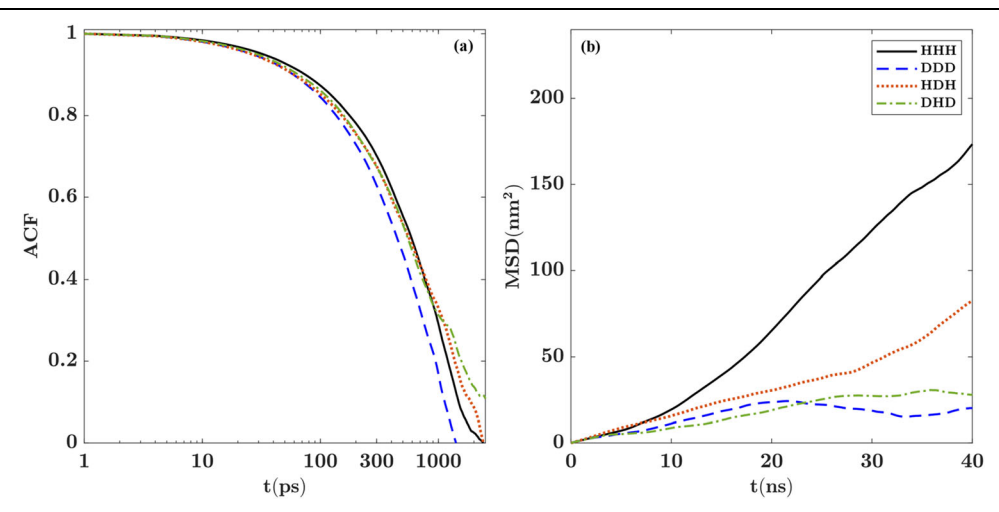


Fig 6. (a) End-to-end distance autocorrelation function of the backbone of the chains. (b) Mean-squared displacement of the polymer chains with respect to their center of mass. In both panels, HHH is shown as a solid line, DDD as a dashed line, HDH as a dotted line, and DHD as a dashed-dotted line.

Structural properties, intermolecular and intramolecular and segment dynamics have been investigated but still the diffusion of the polymers in the solvent has not been discussed. Since polymer chain diffusion is related to the friction force of the solvent and the force is exerted to the outer area of the chain, a meaningful relation can be found between the amount of the SASA and mean-squared displacement (MSD). In this respect, the mean-squared displacement of the single chains is calculated and time-averaged over 50 ns.

The MSD for the different cases is shown in Fig. 6b. Since the MSD of the chains is not linear and does not follow the Fickian diffusion behavior, extracting reliable diffusion coefficients is not straightforward. However, from the MSD, we see that HHH, on average, has traveled the longest distance within the given simulation time while DHD and DDD have moved the least. The MSD of HDH is in between the two cases. The chains with higher H unit content have more diffusion, while higher catechol content leads to a significant decrease of chain diffusion.

DISCUSSION

Hydrophobicity Favors Chain Collapse, Whereas Catechol Groups Hydrate in Water

The hydration analysis using the pair correlation function (Fig. 3) and the number of hydrogen bonds (Table II) between the MIP polar groups and water molecules found that polar backbone groups (ester oxygen and amide nitrogen) do not hydrate and the total number of hydrogen bonds with a polymer chain increases significantly with increasing D unit content. The hydrophobic groups in the backbone and the pendant group of H unit also play a critical role in the final hydrated state of the polymer chain. It is evident from Fig. 4 that both the hydrophobic segments, i.e., in the backbone and H linoleamide side group, engage in hydrophobic interactions and result in the collapse of these MIPs in water. Furthermore, the most collapsed (lowest R_g) polymer (HHH) shows the largest probability of intramolecular hydrogen bonding (Table II) driven by the presence of polar groups in vicinities of each other. The compounded water/ polymer and intra-polymer interactions explain the increasing trend in the radius of gyration with an increase in D unit content. The 2D scatter plot between ${R_g}^2$ and ${R_{\rm ee}}^2$ shows that the polymer with higher D content explores a broader conformational space due to better hydration and hence has higher entropy (a measure of accessible chain conformations). Surprisingly, the 2D scatter plot for R_g^2 versus $R_{\rm ee}^2$ with normalized SASA plotted for every bin (Fig. 5a) illustrates that the SASA correlates with R_g^2 and has no dependence on $R_{\rm ee}^2$. This explains why the $R_{\rm ee}^2$ spans a much broader range compared to that for R_g^2 , as the $R_{\rm ee}^2$ change has relatively no effect on SASA and hence is associated with only a little SASA and hence is associated with only a little energetic penalty. Furthermore, the observation suggests that $R_g^{\ 2}$ increase is associated with a significant energetic penalty (even though the chain entropy increases) as it is correlated with SASA. An increase in SASA can result from either the increase in the number of water-polymer hydrogen bonds (with a simultaneous decrease in intramolecular hydrogen bonds) or the hydration of hydrophobic moieties of the MIPs. Both routes imply an energetic penalty on polymer collapse and hence favor hydration. The increase in SASA with R_g^2 happens with a constant number of water-polymer hydrogen bonds (Fig. 5b), suggesting the hydration through the second route. This presents the notion that comparatively intramolecular hydrogen bonds are stronger (than hydrophobic interactions) and the hydration of the hydrophobic part results in the broadness observed in SASA and R_g^2 .

Why do End-to-end Chain Distance Distributions Show a Peak Around Zero for Co-polymers?

The 2D scatter plots between $R_g^{~2}$ and $R_{\rm ee}^{~2}$ (Fig. 2c) show one of the major populations of polymer chains

with an end-to-end distance around zero. For the case of HDH co-polymer, the population of R_{ee}^2 close to zero is significant as the hydrophobic segment of the two H units collapses (Fig. 4b) to bring the two chain ends in close vicinity. The small value of $R_{
m ee}^{-2}$ distribution is present for DHD polymer as well, which is because the central hydrophobic segment interacts with the hydrophobic segments from the backbone, bringing the hydrophobic segment of D units parallel and close to each other. For the case of HHH polymer, the probability for low $R_{\rm ee}^{-2}$ is minimal as the hydrophobic segment of the first and third units has multiple options for engaging in hydrophobic interactions. Interestingly for the case of the DDD polymer chain, the hydrophobic backbone segments are also collapsed with catechol groups exposed to water but in a fashion in which the hydrophobic segment of the first is parallel to the hydrophobic segment of the second unit, which makes it difficult for the chain ends to interact with each other. This presents an argument that $R_{\rm ee}^{-2}$ might depend upon whether the number of monomers is odd or even for these small MIPs. Note that for polymers with high molecular weight the R_{e^2} might not show any peak around \sim zero. The motivation behind this section was to use $R_{\rm ee}^{\,2}$ as a qualitative descriptor of the polymer chain collapse.

Relations Between Structure and Dynamics

No direct correlation is found between the chain relaxation times and water/polymer or intra-polymer hydrogen bonding numbers, signifying the importance of other interactions such as hydrophobic. The overall chain relaxation time based on the end-to-end distance for the four MIPs (SI, Table II) follows the order: HDH > HHH > DHD > DDD. The relaxation time is highest for the HDH polymer chains as the two hydrophobic side chains are collapsed. In the case of HHH, the polymer relaxes relatively quickly because of the availability of multiple hydrophobic segments. For the case of HDH, even though the first and third unit is H, the relaxation is much slower than the DDD as the central hydrophobic side chain keeps the hydrophobic part of the backbone of the two D units parallel to each other. Interestingly, it is observed that the relaxation of individual units (H and D) of DHD polymer (SI, Table II) is faster than their relaxation in the corresponding homopolymer whereas the overall chain relaxation for DHD polymer is close to that of HHH. This indicates that the chain relaxation for DHD polymer is accompanied by quicker relaxations of individual units resulting in a much broader conformational space evident in the R_g^2 versus $R_{\rm ee}^2$ scatter plot for DHD polymer

It is shown that R_g^2 correlates with SASA, which is consistent with our understanding, i.e., a collapsed chain is less exposed to the solvent and consequently has a lower surface area.

Furthermore, dominant intrachain interactions of the collapsed chains have led to slower chain dynamics, and weak water-polymer interaction makes the chains more isolated. In this respect, the collapsed chains (HHH and HDH) diffuse more like rigid particles than flexible polymer chains.

Connections with Adhesion

Even though it is hard to comment upon the adhesion of these MIPs to a substrate from their solution behavior, we hypothesize some fundamental connections based on the gained knowledge and literature. Thermodynamic work of adhesion is defined as the difference between the free energy of the two materials summed separately and that of their adhered equilibrium state.³⁷ We observe that underwater these MIPs are collapsed because of hydrophobic groups and are hydrating slightly based on catechol groups. The hydrophobic part of such MIPs is known to adsorb in an extended state and result in higher adhesion to hydrophobic substrates underwater. A similar interaction behavior of two hydrophobic segments to the hydrophobic segment/extended hydrophobic surface has been proved earlier.^{38–39} Furthermore, it is found that the benzene ring of the catechol group lies flat on the hydrophobic surfaces to increase the hydrophobic interactions underwater and makes little contribution to adhesion.⁵ Our observation of catechol groups forming multiple hydrogen bonds is important and consistent with the literature. On a hydrophilic substrate, catechol functionality plays a critical role as it engages in multiple hydrogen bonds, hence increasing the probability of the catechol molecule interacting with the substrate. The catechol group prefers a hydrophilic substrate over water as after the formation of a single hydrogen bond through one of a catechol's hydroxyl group, the probability of formation of another hydrogen bond increases because of the vicinities of the substrate to another catechol's hydroxyl group. 14-15 Previously, it has been proven that this probability can be reduced by changing the spacing between surface hydroxyl groups.⁵ The question which intrigues us is whether the presence of hydrophobic groups in the vicinities of a catechol group helps in removing the water from the substrate/catechol interface. Simulating these MIPs on hydrophilic and hydrophobic self-assembled monolayers will be the scope of our future studies.

CONCLUSION

In the last 2 decades, the interest in developing bio-inspired chemistries has increased significantly because of nature's smart all-around approach. Even though the development of mussel-inspired polymers to achieve strong underwater adhesion and their high performance has been achieved, the understanding of the working of these polymers is missing or limited. We scrutinize the structural

behavior and dynamics of mussel-inspired homoand co-polymers of catechol and linoleamide (soybean) side chain-containing monomers. The linoleamide unit of the polymers is engaged in hydrophobic interaction with other hydrophobic side chains or segments in the backbone to result in hydrophobic collapse. The catechol moiety is engaged in a significant amount of hydrogen bonding with water molecules resulting in increased chain size and conformations. Solvent accessible surface area (SASA) has been found to correlate with the radius of gyration but has no dependence on end-to-end distance. The chain relaxation depends on the closeness of different hydrophobic parts of the polymer chain, and the mean-squared displacement of the polymer chains shows a negative trend with an increase in the radius of gyration. These insights into the behavior of MIPs in water would act as a prelude to the enthalpic and entropic factors for the initial state of these polymers when studying their adsorption on a substrate.

ACKNOWLEDGEMENTS

We acknowledge the financial support from the National Science Foundation (NSF) (grant # DMR-1912329, DMR-1610483 and DMR-1508440). The authors would like to thank Amal Narayan and Sukhmanjot Kaur for helpful discussions.

CONFLICT OF INTEREST

On behalf of all authors, the corresponding author states that there is no conflict of interest.

SUPPLEMENTARY INFORMATION

The online version contains supplementary material available at https://doi.org/10.1007/s11837-021-04756-1.

REFERENCES

- 1. K. Kamino, Mar. Biotechnol. 10, 111. (2008).
- R. J. Stewart, T. C. Ransom, and V. Hlady, J. Polym. Sci., Part B: Polym. Phys. 49, 757 (2011).
- 3. J.H. Waite, J. Exp. Biol. 220, 517. (2017).
- H. Zhao, N.B. Robertson, S.A. Jewhurst, and J.H. Waite, J. Biol. Chem. 281, 11090. (2006).
- Z.A. Levine, M.V. Rapp, W. Wei, R.G. Mullen, C. Wu, G.H. Zerze, J. Mittal, J.H. Waite, J.N. Israelachvili, and J.-E. Shea, PNAS USA 113, 4332. (2016).
- W. Wei, J. Yu, C. Broomell, J.N. Israelachvili, and J.H. Waite, J. Am. Chem. Soc. 135, 377. (2013).
- J. Yu, Y. Kan, M. Rapp, E. Danner, W. Wei, S. Das, D.R. Miller, Y. Chen, J.H. Waite, and J.N. Israelachvili, *PNAS USA* 110, 15680. (2013).
- H. Lee, N.F. Scherer, and P.B. Messersmith, PNAS USA 103, 12999. (2006).
- W. Wei, L. Petrone, Y. Tan, H. Cai, J.N. Israelachvili, A. Miserez, and J.H. Waite, Adv. Funct. Mater. 26, 3496. (2016).

- T. Utzig, P. Stock, and M. Valtiner, Angew. Chem Int. 128, 9676. (2016).
- P. Das, and M. Reches, Nanoscale 8, 15309. (2016). 11.
- Y. Li, H. Liu, T. Wang, M. Qin, Y. Cao, and W. Wang, ChemPhysChem 18, 1466. (2017).
- J. Wang, M.N. Tahir, M. Kappl, W. Tremel, N. Metz, M. Barz, P. Theato, and H.J. Butt, Adv. Mater. 20, 3872. (2008).
- S.A. Mian, L.C. Saha, J. Jang, L. Wang, X. Gao, and S. Nagase, *J. Phys. Chem. C.* 114, 20793. (2010).
- S.A. Mian, X. Gao, S. Nagase, and J. Jang, Theor. Chem. Acc. 130, 333. (2011).
- P. Redfern, P. Zapol, L. Curtiss, T. Rajh, and M. Thurnauer, J. Phys. Chem. B. 107, 11419. (2003).
- 17. I.-C. Yeh, J.L. Lenhart, J.A. Orlicki, and B.C. Rinderspacher, J. Phys. Chem. B. 123, 7024. (2019).
- I.-C. Yeh, J.L. Lenhart, and B.C. Rinderspacher, J. Phys. 18. Chem. C. 119, 7721. (2015).
- G. Westwood, T.N. Horton, and J.J. Wilker, Macromolecules 40, 3960. (2007).
- 20. H. Xu, J. Nishida, W. Ma, H. Wu, M. Kobayashi, H. Otsuka, and A. Takahara, ACS Macro Lett. 1, 457. (2012).
- J. Yang, M.A.C. Stuart, and M. Kamperman, Chem. Soc. Rev. 43, 8271. (2014).
- K. Kendall, J. Adhes. 5, 179. (1973).
- S. Kaur, A. Narayanan, S. Dalvi, Q. Liu, A. Joy, A. Dhinojwala, and A.C.S. Cent, Sci. 4, 1420. (2018).
- A. Narayanan, S. Kaur, C. Peng, D. Debnath, K. Mishra, Q. Liu, A. Dhinojwala, and A. Joy, Biomacromol 20, 2577. (2019).
- 25. $Material\ Studio^{TM}$, by Dassault Systèmes BIOVIA, UK (Accelrys®), (License purchased by The University of Ak-

- 26. L. Martínez, R. Andrade, E.G. Birgin, and J.M. Martínez, J. Comput. Chem. 30, 2157. (2009).
- W. Damm, A. Frontera, J. Tirado-Rives, and W.L. Jor-
- gensen, J. Comput. Chem. 18, 1955. (1997). W.L. Jorgensen, D.S. Maxwell, and J. Tirado-Rives, J. Am. 28. Chem. Soc. 118, 11225. (1996).
- 29. H. Berendsen, J. Grigera, and T. Straatsma, J. Phys. Chem. 91, 6269. (1987).
- 30. S. Plimpton, J. Comput. Phys. 117, 1. (1995).
- M. Rubinstein, and R. H. Colby, Polymer Physics; Oxford university press New York, 2003; Vol. 23.
- D. Chandler, and J.K. Percus, *Phys. Today.* 41, 114. (1988).
 - A. Luzar, and D. Chandler, J. Chem. Phys. 98, 8160. (1993).
- N. Kumar, S. Singla, M.C. Wilson, S. Kaur, S. Bekele, M. Tsige, and A. Dhinojwala, J. Phys. Chem. C. 123, 29729. (2019)
- 35. D. Chandler, Nature 437, 640. (2005).
- G. Williams, and D.C. Watts, J. Chem. Soc. Faraday Trans. 66, 80. (1970).
- 37. A. Dupré, and P. Dupré, Théorie Mécanique De La Chaleur; Gauthier-Villars, 1869.
- N.B. Rego, E. Xi, and A.J. Patel, J. Am. Chem. Soc. 141, 38. 2080. (2019).
- S. Vembanur, A.J. Patel, S. Sarupria, and S. Garde, J. Phys. 39. Chem. B. 117, 10261. (2013).

Publisher's Note Springer Nature remains neutral with regard to jurisdictional claims in published maps and institutional affiliations.